# Moon and Sun shadowing effect in the MACRO detector

M. Ambrosio [ℓ], R. Antolini [g], A. Baldini [m], G. C. Barbarino [ℓ], B. C. Barish [d], G. Battistoni [f,u], Y. Becherini [b], R. Bellotti [a], C. Bemporad [m], P. Bernardini [j], H. Bilokon [f], C. Bower [h], M. Brigida [a], S. Bussino [r], F. Cafagna [a], M. Calicchio [a], D. Campana [ℓ], M. Carboni [f], R. Caruso [i], S. Cecchini [b,v], F. Cei [m], V. Chiarella [f], T. Chiarusi [b], B. C. Choudhary [d], S. Coutu [k,ab], M. Cozzi [b], G. De Cataldo [a], H. Dekhissi [b,q], C. De Marzo [a], I. De Mitri [j], J. Derkaoui [b,q], M. De Vincenzi [s], A. Di Credico [g], O. Erriquez [a], C. Favuzzi [a], C. Forti [f], P. Fusco [a], G. Giacomelli [b], G. Giannini [m,w], N. Giglietto [a,*], M. Giorgini [b], M. Grassi [m], A. Grillo [g], C. Gustavino [g], A. Habig [c,ag], K. Hanson [k], R. Heinz [h], E. Katsavounidis [d,ah], I. Katsavounidis [d,ai], E. Kearns [c], H. Kim [d], A. Kumar [b], S. Kyriazopoulou [d], E. Lamanna [n,ac], C. Lane [e], D. S. Levin [k], P. Lipari [n], N. P. Longley [d,aa], M. J. Longo [k], F. Loparco [a], F. Maaroufi [b,q], G. Mancarella [j], G. Mandrioli [b], S. Manzoor [b,ae], A. Margiotta [b], A. Marini [f], D. Martello [j], A. Marzari-Chiesa [p],

M. N. Mazziotta [a], D. G. Michael [d], P. Monacelli [i],

T. Montaruli [a], M. Monteno [p], S. Mufson [h], J. Musser [h],

D. Nicolò [m], R. Nolty [d], C. Orth [c], G. Osteria [ℓ], O. Palamara [g],

L. Patrizii [b], R. Pazzi [m], C. W. Peck [d], L. Perrone [j], S. Petrera [i],

V. Popa [b,z], A. Rainò [a], J. Reynoldson [g], F. Ronga [f],

C. Satriano [n,t], E. Scapparone [g], K. Scholberg [c,ah], M. Sioli [b],

G. Sirri [b], M. Sitta [p,af], P. Spinelli [a], M. Spinetti [f], M. Spurio [b],

R. Steinberg [e], J. L. Stone [c], L. R. Sulak [c], A. Surdo [j], G. Tarlè [k],

V. Togo [b], M. Vakili [o,aj], C. W. Walter [c], R. Webb [o]

[a] *Dipartimento Interateneo di Fisica del Politecnico-Università di Bari and INFN, 70126 Bari, Italy*

[b] *Dipartimento di Fisica dell'Università di Bologna and INFN, 40126 Bologna, Italy*

[c] *Physics Department, Boston University, Boston, MA 02215, USA*

[d] *California Institute of Technology, Pasadena, CA 91125, USA*

[e] *Department of Physics, Drexel University, Philadelphia, PA 19104, USA*

[f] *Laboratori Nazionali di Frascati dell'INFN, 00044 Frascati (Roma), Italy*

[g] *Laboratori Nazionali del Gran Sasso dell'INFN, 67010 Assergi (L'Aquila), Italy*

[h] *Depts. of Physics and of Astronomy, Indiana University, Bloomington, IN 47405, USA*

[i] *Dipartimento di Fisica dell'Università dell'Aquila and INFN, 67100 L'Aquila, Italy*

[j] *Dipartimento di Fisica dell'Università di Lecce and INFN, 73100 Lecce, Italy*

[k] *Department of Physics, University of Michigan, Ann Arbor, MI 48109, USA*

[ℓ] *Dipartimento di Fisica dell'Università di Napoli and INFN, 80125 Napoli, Italy*

[m] *Dipartimento di Fisica dell'Università di Pisa and INFN, 56010 Pisa, Italy*

[n] *Dipartimento di Fisica dell'Università di Roma "La Sapienza" and INFN, 00185 Roma, Italy*

[o] *Physics Department, Texas A&M University, College Station, TX 77843, USA*

[p] *Dipartimento di Fisica Sperimentale dell'Università di Torino and INFN, 10125 Torino, Italy*

[q] *L.P.T.P, Faculty of Sciences, University Mohamed I, B.P. 524 Oujda, Morocco*

[r] *Dipartimento di Fisica dell'Università di Roma Tre and INFN Sezione Roma Tre, 00146 Roma, Italy*

[s] *Dipartimento di Ingegneria dell'Innovazione dell'Università di Lecce and INFN 73100 Lecce, Italy*

[t] *Also Università della Basilicata, 85100 Potenza, Italy*

[u] *Also INFN Milano, 20133 Milano, Italy*

[v] *Also Istituto TESRE/CNR, 40129 Bologna, Italy*

[w] *Also Università di Trieste and INFN, 34100 Trieste, Italy*

[x] *Also Dipartimento di Energetica, Università di Roma, 00185 Roma, Italy*

[y] *Also Institute for Nuclear Research, Russian Academy of Science, 117312 Moscow, Russia*

[z] *Also Institute for Space Sciences, 76900 Bucharest, Romania*

[aa] *Macalester College, Dept. of Physics and Astr., St. Paul, MN 55105*

[ab] *Also Department of Physics, Pennsylvania State University, University Park, PA 16801, USA*

[ac] *Also Dipartimento di Fisica dell'Università della Calabria, Rende (Cosenza),*

*Italy*

[ad] *Also Department of Physics, James Madison University, Harrisonburg, VA 22807, USA*

[ae] *Also RPD, PINSTECH, P.O. Nilore, Islamabad, Pakistan*

[af] *Also Dipartimento di Scienze e Tecnologie Avanzate, Università del Piemonte Orientale, Alessandria, Italy*

[ag] *Also U. Minn. Duluth Physics Dept., Duluth, MN 55812*

[ah] *Also Dept. of Physics, MIT, Cambridge, MA 02139*

[ai] *Also Intervideo Inc., Torrance CA 90505 USA*

[aj] *Also Resonance Photonics, Markham, Ontario, Canada*

[ak] *Also Department of Physics, SLIET,Longowal,India*

---

**Abstract**

Using data collected by the MACRO experiment from 1989 to the end of its operations in 2000, we have studied in the underground muon flux the shadowing effects due to both the Moon and the Sun. We have observed the shadow cast by the Moon at its apparent position with a significance of 6.5 $\sigma$. The Moon shadowing effect has been used to verify the pointing capability of the detector and to determine the instrument resolution for the search of muon excesses from any direction of the celestial sphere. The dependence of the effect on the geomagnetic field is clearly shown by splitting the data sample in day and night observations. The Sun shadow, observed with a significance of 4.6 $\sigma$ is displaced by about 0.6° from its apparent position. In this case however the explanation resides in the configuration of the Solar and Interplanetary Magnetic Fields, which affect the propagation of cosmic ray particles between the Sun, and the Earth. The displacement of the Sun shadow with respect to the real Sun position has been used to establish an upper limit on

the antimatter flux in cosmic rays of about 48% at 68% c.l. and primary energies of about 20 TeV.

*Key words:* MACRO; underground muons;Moon shadowing; Sun shadowing; geomagnetic field; IMF field; primary antimatter

*PACS:* 13.85.Tp, 96.40.-z, 96.40.Cd, 96.40.De, 96.40.Tv, 96.50.Bh

## 1 Introduction

MACRO was a large area underground detector located in Hall B of the Gran Sasso National Laboratory (LNGS) in Italy at an average depth of 3700 m.w.e, 13° 34´ E longitude and 42° 27´ N latitude. A detailed description of the detector can be found in [1]. The experiment was primarily designed to search for monopoles and rare particles in the cosmic rays, including high energy neutrinos and muons from cosmic point sources [2]. These sources can be inferred from an excess of muons above a nearly isotropic background in a particular region of the sky [3,4]. An important requirement for any kind of detector using this technique is the determination of the best signal/background ratio, which is related to the angular resolution.

It was originally suggested by Clark [5] that an observed narrow angle "shadow" in the cosmic ray flux due to the absorption by the Sun and the Moon can be useful to test the angular resolution[6] and the pointing ability of cosmic ray detectors[3,4]. Moreover, the positive determination of the Moon shadow in the expected position, validates the analyses of coincident

* Corresponding author.

*E-mail address:* giglietto@ba.infn.it

data between different detectors as MACRO together EAS-TOP[7] or other detectors[8].

However, since the angular diameter of these bodies is about 0.5° wide, only detectors having good angular resolution and sufficient statistics have the possibility to detect this signal. Several large air shower arrays [9–15] and shallow depth detectors [16] have observed these effects. Deep underground observations (>2000 m.w.e.) have greater difficulties in observing the shadows, due to the greatly reduced underground muon flux. However MACRO [17], SOUDAN2 [18] and LVD [19] have all collected data continuously for about 10 years, thereby gaining the sufficient sensitivity to observe the effect.

Underground muons are the remnants of the air showers initiated by the collisions of primary cosmic rays with air nuclei. The secondary muons which reach the MACRO detector had to cross a minimum rock overburden of 3200 hg cm$^{-2}$. This corresponds to a minimum energy of the muon at the surface of about 1.4 TeV and to a primary proton with median energy around 22 TeV. Since the Earth Magnetic field is approximately (to within 10%) a dipole field, and its strength is 0.5 G at the surface, a single charged particle crossing it will acquire a transverse momentum of about 25 GeV/c for a path integral over few Earth' radii. The average displacement of muon trajectories due to this effect,as viewed in the detector, will be $[0.15^\circ\ Z/(E_p/10\ TeV)]$, eastward for positive primaries, [20,21]. Therefore the apparent position of the Moon shadow will appear moved to the west direction (with respect to the Earth-Moon direction) by the same amount.

The motion in time of the Earth's magnetic pole around its average position, introduces a smearing of the shadow when the effect is observed over

many years [22]. Additional smearing can be produced by the fact that the observations are made at different angles and at different times of the year.

The Sun shadowing effect is more complicated to estimate. Particles shadowed by the Sun are traveling in the direction of the Sun-Earth axis and therefore are traveling through the solar magnetic field and the Interplanetary Magnetic Field (IMF). The IMF is due to the electric currents in the Sun that generate a complex magnetic field which extends out into the interplanetary space. As the Sun's magnetic field is carried out through the solar system by the solar wind and the Sun is rotating, the rotation winds up the magnetic field into a large rotating spiral, known as the Parker spiral. The magnetic field is primarily directed outward from the Sun in one of its hemispheres, and inward in the other. This causes opposite magnetic field directions in the Parker spiral. The thin layer between the different field directions is described as the neutral current sheet. Since this dividing line between the outward and inward field directions is not exactly on the solar equator, the rotation of the Sun causes the current sheet to become "wavy", and this waviness is carried out into interplanetary space by the solar wind. For this reason the IMF shows a sector structure with field directions reversing across the sector boundaries [23,24]; therefore, in some sectors the magnetic field points inward, and outward in others. Moreover, this structure varies with the solar activity cycle; a complete simulation must thus take into account the solar activity phase and the sectors encountered by the particle traveling in our solar system[25–27].

The possibility to use the Moon and Sun shadows as mass spectrometers was first explored by Lloyd-Evans [28]; following this idea Urban et al. [20] proposed this method as a way to search for antimatter in primary cosmic rays. If there is a significant antimatter component in the primary CRs

in the TeV energy region, then the magnetic fields should deflect them in opposite direction with respect to the matter component; therefore the proton component should be deflected by the geomagnetic field eastward and the antiproton component westward. As a consequence the shadow produced by the proton component should be to the west with respect to the Moon center, while the resulting shadow due to antiprotons should be to the east. However to resolve the images, the two disks must be far from each other, at least by the disk diameter itself.

The shadow of the Moon was previously observed by MACRO using a partial data sample[17]. In this paper we present the measurement of the Moon and Sun shadows using the full data set of muons collected by the MACRO detector. Using the result obtained for the Sun we are able to set an upper limit to the antiproton flux of TeV energy at the Earth.

## 2 The muon data sample and the expected background

### *2.1 Muon data sample*

The muon sample used for the present analysis includes all events collected from the start of MACRO data taking in February, 1989 through the end of 2000. The sample totals $50.0 \times 10^6$ events collected over 74,073 hours of livetime. During the first part of this period, the apparatus was under construction. The three main detector configurations included one ($A_{eff}\Omega \approx 1,010$ m$^2$ sr) and six ($A_{eff}\Omega \approx 5,600$ m$^2$ sr) supermodules without the attico (the upper part of the detector described in[1]), and finally the full six supermodules with attico ($A_{eff}\Omega \approx 6,600$ m$^2$ sr). Approximately 60% of the

data sample was obtained during periods when MACRO had full acceptance.

The run and event was used to select good quality events were the same as in our first analysis of the Moon shadow [17] and for the muon-astronomy searches [3]. Thus, only muon events contained in a half-angle cone of 10° and centered on the Moon and the Sun have been retained for further analysis. The number of events that passed all cuts in the Moon window was 404988, almost doubling the previous statistics, and 396662 events in the Sun window. The rate of accumulation of the events in the two windows is given in Fig. 1. As visible in Fig. 1 the effects of a reduced detector livetime, due to the installation of the final configurations in years 1992-1993, produced a different esposure for the Sun and The Moon.

We note that during the period when MACRO was operative the solar activity went from its maximum phase in 1991, through a minimum phase around 1996/97 to the beginning of the next maximum in 2001. However almost 62% of the total events were accumulated from 1994 onward, close to the period of minimum solar activity when the neutral sheet was probably lying close to the ecliptic plane with little warping [29]. The period is contained within the so-called A>0 phase of the solar cycle during which the magnetic field of the Sun is directed outward at the north pole of the Sun and inward in the South.

As in our previous analysis, for each real event observed, we produced 25 simulated background events, by randomly coupling muon directions and times, as explained in [3]. This technique was used to estimate the expected events from any direction of the sky, including the Sun and the Moon.

## 3 Shadow of the Moon

The Moon is a celestial body moving quickly in the sky. Thus, to perform the analysis it is necessary to make a very precise and accurate computation of its position. The topocentric position of the moon was computed at the arrival time of each event using the database of ephemerides available from the Jet Propulsion Laboratory, JPLEPH [30]. A correction for the parallax due to MACRO's instantaneous position on the Earth was then applied to each ephemeris position [31].

### *3.1 Event deficit around the Moon*

The distribution of events with arrival directions close to the Moon direction can be used to make visible the event deficit around the Moon disk. The average disk radius is computed for each event of the 404988 events in the sample giving a value of $0.26 \pm 0.01$. Fig. 2 shows the distribution $\frac{1}{\pi}\frac{dN}{d\theta^2}$vs.$\theta$, where $\theta$ is the angular distance between the calculated Moon center position in celestial coordinates and the muon arrival direction. The significance of the deficit can be calculated by fitting this distribution with a function of the form [9,32]:

$$\frac{dN_\mu}{d\theta^2} = k(1 - \frac{\theta_M^2}{2\sigma^2} e^{-\frac{\theta^2}{2\sigma^2}}) \tag{1}$$

where $\theta_M = 0.26^\circ$ is the average value of the angular radius of the Moon, previously computed, $\sigma$ is the detector angular resolution and k the event density.

This function represents the signal produced by the Moon absorption effect when the detector point spread function (PSF) can be assimilated to a bidimensional normal distribution. We know that in our case this is not really appropriate because muons observed in the apparatus undergo multiple Coulomb scattering in the overburden rock, which generates long tails in the measured angular distributions. Nonetheless, this simple analysis gives results consistent with the one presented in the next section where we take into account the real PSF of the apparatus by using a maximum likelihood method. The fit of the data to the above function has a $\chi^2 = 54.8$ for 31 D.o.F. and a $\chi^2 = 95.9$ for a flat distribution (32 D.o.F.). The difference between these values suggests that the chance probability of the observed deficit is $\leq 10^{-9}$, equivalent to a statistical significance of about $6\sigma$. The fitted values of the parameters are $\mathrm{k} = (1294 \pm 5)$ events/degree$^2$ and $\sigma = (0.55 \pm 0.05)^\circ$ . The value of k obtained by the fit can be used to have a rough estimate of the number of missing events (blocked by the Moon disk): $\pi \mathrm{k} \cdot \theta_{\mathrm{M}}^2 = 275 \pm 1$. We also estimated the number of missing events by considering the number of expected background events in the $10^\circ$ cone windows, $\mathrm{N}_{bck} = 405100 \pm 127$, calculated as mentioned above. Thus, the number of blocked events is $405100 \cdot (\frac{0.26^\circ}{10^\circ})^2 = 274 \pm 1$, in agreement with the result of the fit. Since the livetime of the apparatus for the entire sample is about 74000 hr, the rate of the events obscured by the Moon is about 3 events/month.

The observed signal can then be used to optimize the bin size for astronomy searches [3]. In fact we can choose the size of a circular window centered on the Moon that maximizes the statistics $\frac{N_{exp}-N_{obs}}{\sqrt{N_{exp}}}$, being $N_{obs}$ integrated the number of events observed in the Moon direction and $N_{exp}$ the integrated

number of expected events in the same direction. The behavior of this quantity versus the angular distance from the Moon center, is shown in Fig.3. This figure suggests the choice of bin 0.5° radius wide as the optimal one for maximizing the signal if there is a source at the center of the bin [3].

### *3.2 Maximum likelihood analysis*

In the simple one dimensional analysis above, we have implicitly assumed that the position of the moon's shadow is known and the significance calculated as the PSF of the apparatus is a perfect two dimensional normal distribution. However geomagnetic effects, displacement of the shadow and the distortions introduced by the true PSF, cannot be easily taken into account using this analysis. For all these reasons we have developed a binned likelihood method, based on a *a priori* knowledge of the MACRO PSF (MPSF), a technique originally developed by COS-B[33].

The MPSF was accurately determined by using double muon events in the detector. Muon pair events are produced in the decays of pions and kaons produced in the primary cosmic ray interactions; these muons therefore come from about 20 km above the apparatus and have small initial separation angles; thus they reach the apparatus with almost parallel paths. Therefore, the distribution of their separation angles is a good measurement of convolution of the scattering in the mountain overburden and the detector's intrinsic angular resolution. This space angle should be divided by a factor $\sqrt{2}$ to take into account of the independent deviations of each muon in the pair. The reconstructed MPSF [17] is more peaked to small angular deviations, with

respect to a normal distribution, but with long tails at large deviations.

In order to analyze both the Moon and the Sun shadowing effects, we have to take into account the finite size of these objects. Therefore we have modified the true MPSF by selecting random positions on a disk having the same angular dimensions of the Moon and then generating random deviations according the MPSF. This new distribution, a convolution of the original MPSF and an extended source of fixed angular radius, is then used as the PSF for the analysis. The sensitivity of the results to the angular radius of the object will be explored at the end of this section.

A two dimensional likelihood analysis was performed, composing the observed data with the expectation from a source of unknown strength and position. We filled a two-dimensional histogram, centered on the Moon position, and a similar histogram containing the simulated events, obtained by adding to the expected background [3], the events due to a source at $(x_s, y_s)$ having a chance strength $S_M$, spread according to the modified PSF. The source in this case should have negative strength, since we are looking for an attenuation. Both the observed and simulated events are plotted using horizontal coordinates (azimuth and altitude) and using equal solid angle bin ($\Delta\Omega = 0.125^\circ \times 0.125^\circ = 1.6 \times 10^{-2}$ deg$^2$). For each of the bin in the histogram used, we assume to have a source exactly at the bin center, then the unknown strength $S_M$ is evaluated by minimizing the quantity $\chi^2$ for poissonian distributed data [34]

$$\chi^2(x_s, y_s, S_M) = 2 \sum_{i=1}^{n_{bin}} [N_i^{sim} - N_i + N_i \ln \frac{N_i}{N_i^{sim}}], \quad (2)$$

where the sum is over all bins in the window [34], $N_i$ is the observed number of muons in the i-th bin, and $N_i^{sim}$ the number of events in the same bin from the simulated distribution. The minimum value found in each bin, $\chi^2(x_s, y_s, S_M)$ was then compared with $\chi^2(0)$ for the *null hypothesis* that no shadowing source is present at the center of the bin ($S_M = 0$). We then fill a new two-dimensional histogram filled with the quantity $\lambda = \chi^2(0) - \chi^2(x_s, y_s, S_M)$. The most likely position of the Moon shadow is given by the bin having the maximum value $\lambda^{max} \equiv \Lambda$. Since there is only one free parameter, the strength of the source $S_M$, $\lambda$ behaves like $\chi^2_1$, a $\chi^2$ distribution with one degree of freedom [33]. The significance of the moon detection is given by $\mathrm{P}(\chi^2_1 \geq \chi^2_1(\Lambda))$.

In Figure 4 we show the results of this analysis in a window $4.375^\circ \times 4.375^\circ$ centered on the moon position. This window has been divided into $35 \times 35$ cells, each having dimensions $0.125^\circ \times 0.125^\circ$. The $\lambda$ values of this figure are displayed in grey scale format for every bin in the moon window. Also shown is the fiducial position of the Moon and a circle centered at this position corresponding to the average lunar radius, $0.26^\circ$. The largest deviation away from the expected background is found at $(0.^\circ\ , +0.125^\circ\ )$ with a $\Lambda = 39.1$, corresponding to a significance of $6.5\sigma$ and a negative strength of 316 events, as expected for a shadowing effect. The $\chi^2$ value for the null hypothesis, i.e. when a source of null intensity is set in the bin with the largest deviation found, is 1240.71 for the $35 \times 35$ bins. The entire sky region in the fiducial position of the disk has $\lambda \geq 36.$ values. Moreover the negative strength observed is equal to $316 \pm 40$ events, in agreement with the expected deficit. The $1\sigma$ error in the strength, treated as a parameter, is directly estimated by the likelihood method by considering the parameter interval delimited by the

condition $\lambda = \Lambda - 1$[34] (or $\chi^2 = \chi^2_{min} + 1$).

We estimated other parameters used in the simulation, like the Moon average radius [13], in order to verify the correctness of the analysis or the MPSF shape itself [17]. For this consideration we assume that the true shadow center position is that having the largest deviation, i.e. at ($0.^\circ$ ,$+0.125^\circ$ ), and repeat the analysis using different PSFs each modified by different values of the trial angular radius for the source, starting with a null value corresponding to the true, unmodified MPSF. This technique let us to both verify the sensibility of the analysis to extended PSFs and also to quote an error on the radius of the measured object. Fig.5 shows the $\chi^2$ values at the central shadow position, versus the trial angular disk radius. From this figure we can quote as the radius for the Moon a value of $(0.25 \pm 0.25)^\circ$ , well in agreement with the correct averaged value. This result confirms that the Moon shadow signal is more likely due to an extended source instead of a point-like source.

The displacement of the shadow is in good agreement with the expected position, and this confirms the correct alignment of the apparatus. We can quote as the maximum error in the alignment of the apparatus a value of about $0.1^\circ$, taking into account the observed shadow displacement northward.

## 4 Day-Night effects

To study possible differences in the geomagnetic field due to the solar wind, we divided the muon sample in two subsamples by requiring that the angular

distance between the Moon and the Sun is smaller or larger than 90°. This requirement is almost equivalent to a daytime-nighttime requirement on the data, similar to what was used in a previous analysis [35]. The results of the analyses for the two subsamples are shown in Fig.6a-b: there is a sharper shadow for the "night" sample, with a large significance, and a broader shadow for the "day" sample (with a lower significance). Since the two subsamples are almost equivalent (198183 and 206805 events for "day" and "night" respectively) we conclude that night events encounter a reduced geomagnetic field with respect to the day events [36–38]. The cause has probably to be ascribed to the different configuration of the geomagnetic field in the two sides. Also time varying effects can be different for the two subsamples.

## 5 Shadowing effect of the Sun

The same analysis was performed also for the Sun. In this case the total number of events collected with an angular distance from the Sun center of 10° is 396662, a sample almost equivalent to that of the Moon. Since the angular dimensions of the two bodies are essentially the same, we expect about the same number of missing events. However, besides the geomagnetic field effect, two other magnetic fields come into deflecting the cosmic ray particles: the Sun's magnetic field and the IMF. As these fields are variable in time, it is more difficult to predict the shadow displacement. Using the ecliptic coordinates for the muons collected, and a window centered on the calculated Sun position, we obtain the results shown in Fig. 8. The deficit is clear and it is displaced by 0.6° northward with a $\chi^2 = 22.0$ corresponding to a signal significance of 4.6 $\sigma$. The deficit observed for the Sun shadowing results to

be $247 \pm 48$ events, using the error estimated by the likelihood method as for the Moon shadowing effect. In trying to explain our result let us analyze the behavior of the magnetic fields in the years during which we collected our data. Fig. 7 shows the monthly average $A_p$ values [39] in the years 1989-2000. These values indicate a global (planetary) magnetic activity and are sensitive to solar particle effects on the Earth's magnetic field. It is evident that the Sun was in a relatively quiet activity during 1993-2000, where the bulk of our events have been collected. Moreover, as we have mentioned in section 2.1, during the whole period the solar cycle was in the so-called A>0 phase. In this situation the displacement due to the large regular IMF is expected to be northward of the ecliptic plane. Let us note that from 1991 till the end of 1997 the Heliospheric Current Sheet was estimated to have a tilt angle $<25^\circ$ and was almost symmetric between the north and south hemispheres of the solar cavity.

Since MACRO is located at a high latitude, it is possible that by averaging over a long period of observations the net result produces a displacement to the north as if the apparatus was mostly looking in the "away" hemisphere of the IMF. The amplitude and the direction of the shift is in agreement with other observations at the same energy range[40,41].

## 6 Antiproton flux limits

The displacement of the Sun shadow from the expected center position can be used to evaluate a limit on the antiproton abundance in the cosmic ray flux [20,42,22]. In fact if a primary antiproton flux is present, it should produce a displacement on the opposite direction with respect to that of the proton

flux [20]. The $\chi^2$ level in the symmetric position with respect to the sun center, i.e. at 0.6° southward, results to be $\chi^2 = 3.2$. In this case we use again the likelihood analysis to estimate an upper limit at the desired confidence level. Taking into account that the $\lambda$ variable follows the $\chi^2$ distribution with one degree of freedom, we can estimate the upper limit at 68% c.l. choosing $\Delta\chi^2 = 1$ and the upper limit at 90% c.l. choosing to $\Delta\chi^2 = 2.7$. Using this method we obtain $n_{68\%} = 125$ events and $n_{90\%} = 155$ events of deficit. Therefore $\overline{\mathrm{p}}/\mathrm{p} = 51\%$ at 68% c.l. and $\overline{\mathrm{p}}/\mathrm{p} = 62\%$ at 90% c.l. for primaries at a mean energy of about 20 TeV [35]. We can also evaluate the upper limit looking to the event density distributions centered in the position found for the sun shadow, i.e. 0.6° displaced northward respect to the Sun "nominal" position, and in the symmetric position. The two distributions are shown in Fig.9, and again is visible the deficit in the distribution northward position while the other is flat. Using the considerations derived from Fig.3 we found that the number of observed events within 0.5°, from the distribution southward centered, gives 664 events observed and 710 expected. We can therefore quote the upper limit as 60 events (68%c.l.) and 81 events (90%c.l.).

Since as previously explained[3] the choice of a 0.5° half-angle cone, collects about 50% of events from a source, the upper limit should be $\overline{\mathrm{p}}/\mathrm{p} = 120/247 = 48.5\%$ at 68%c.l. and $\overline{\mathrm{p}}/\mathrm{p} = 162/247 = 52.\%$ at 90%c.l. in agreement with the likelihood estimations.

Figure 10 shows our $\overline{\mathrm{p}}/\mathrm{p}$ limit compared to measurements from other experiments.

## 7 Conclusions

Using a sample of 50 million muons MACRO has detected the Moon and Sun shadows, with a significance of 6.5 and 4.6 $\sigma$, respectively. The strength of the signals is in agreement with those expected. The Moon shadow effect is centered as expected in the case of primary protons of 15 TeV energy (median), demonstrating the correctness and the stability of the detector pointing ability. The Sun shadow is shifted with respect to the "nominal" center position. The absence of a symmetric shadow leads to an upper limit of the $\overline{\mathrm{p}}/\mathrm{p}$ ratio of 48.5% at 68% c.l. for high energy cosmic rays. MACRO is the deepest detector to observe the shadows of the Sun and of the Moon. This investigation confirms that the apparatus had the capability to detect signals from cosmic sources by observing secondary muons underground[3,4].

## 8 Acknowledgments

We gratefully acknowledge the support of the director and of the staff of the Laboratori Nazionali del Gran Sasso and the invaluable assistance of the technical staff of the Institutions participating in the experiment. We thank the Istituto Nazionale di Fisica Nucleare (INFN), the U.S. Department of Energy and the U.S. National Science Foundation for their generous support of the MACRO experiment. We thank INFN, ICTP (Trieste), WorldLab and NATO for providing fellowships and grants (FAI) for non Italian citizens.

## References


[1] S. P. Ahlen *et al.* (MACRO Collaboration), Nucl. Instrum. Meth. **A324** (1993) 337; M. Ambrosio *et al.*(MACRO Collaboration), Nucl. Instrum. Meth., **A486** (2002) 663

[2] M. Ambrosio *et al.*(MACRO Collaboration), hep-ex/0206027

[3] S.Ahlen et al.(MACRO Collaboration), Astrophys. J. **412** (1993) 301; M. Ambrosio *et al.*(MACRO Collaboration),Astrop. Phys. **18** (2003), 615.

[4] M. Ambrosio *et al.* (MACRO Collaboration), Astrophys. J. **546** (2001) 1038.

[5] G.W. Clark, Phys. Rev. **108** (1957) 450.

[6] M. Merck *et al.*, Astrop. Phys. **5** (1996), 379.

[7] M. Aglietta *et al.* (MACRO-EAS TOP Collaborations), Phys. Lett. B, **337** (1994) 376; Phys. Rev. D **42**, (1990) 1396.

[8] M. Ambrosio *et al.,* (MACRO-GRACE Collaborations), Phys. Rev. D **50** (1994) 3046.

[9] D.E. Alexandreas *et al.*, Phys. Rev. D **43** (1991) 1735.

[10] P.L. Ghia *et al.*, Proc. 26th Rencontres de Moriond (O. Fackler, G. Fontaine, J. Trân Thanh Vân Eds.), Edition Frontiéres, 1991, 217; Proc. 22nd ICRC (Dublin, 1991) vol. 2, 708.

[11] A. Karle *et al.*, Proc. 22nd ICRC (Dublin, 1991) vol. 4, 460.

[12] M. Amenomori *et al.*, Phys. Rev. D **47** (1993) 2675.

[13] A. Borione *et al.*, Phys. Rev. D **49** (1994) 1171.

[14] F. Samuelson *et al.*, Proc. 27th ICRC (Hamburg, 2001) vol. 2, 594.

[15] B. Bartoli *et al.*, Nuovo Cim. **24C** (2001) 669.

[16] J. Parriaud (L3 Collaboration), to be published on the Proc. of XIVth Rencontres de Blois (2002), arXiv:astro-ph/0210334.

[17] M. Ambrosio *et al.* (MACRO Collaboration), Phys. Rev. D **59** (1999) 012003; N. Giglietto *et al.* (MACRO Collaboration), Proc. 26th ICRC (Salt Lake City, 1999) vol. 7, 214.

[18] J.H. Cobb *et al.*, Proc. 26th ICRC, (Salt Lake City, 1999) vol. 7, 230.

[19] M. Aglietta *et al.* (LVD Collaboration), Proc. 26th ICRC (Salt Lake City, 1999) vol. 7, 22.

[20] M. Urban *et al.* Nucl. Phys. Proc. Suppl. **14B** (1990) 223.

[21] J. Heintze *et al.*, MPI-H-1989-V7 and Proc. 21st ICRC (Adelaide, 1990) vol. 4, 456.

[22] D. Pomaréde *et al.*, Astrop. Phys. **14** (2001) 287.

[23] J.M. Wilcox and N.F. Ness, J. Geophys. Res., **70** (1965), 5783.

[24] L. Svalgaard and J.M. Wilcox, Ann. Rev. Astron. Astrophys., **16** (1978) 429

[25] M. Onhishi et al., Proc 22nd ICRC (Dublin, 1991) vol. 2, 69.

[26] T. Zhang and J. Mu, Proc 26th ICRC (Salt Lake City, 1999) vol. 7, 210.

[27] Y. Suga et al., Proc 26th ICRC (Salt Lake City, 1999) vol. 7, 202.

[28] J. Lloyd-Evans, Proc. 19th ICRC, (La Jolla, 1985) vol. 2, 173.

[29] A. Balogh and E.J. Smith, Space Sci. Rev., **97** (2001) 147.

[30] E.M. Standish *et al.*, "JPL Planetary and Lunar Ephemerides", JPL IOM **314** (1995) 10.

[31] P. Duffett-Smith, "Practical Astronomy with your Calculator", 3rd ed. (Cambridge University Press, 1988), p.150.

[32] J.H. Cobb *et al.*, Phys. Rev. D **61** (2000) 092002.

[33] A.M.T. Pollock *et al.*, Astron. Astrophys. **94** (1981) 116.

[34] D.E. Groom *et al.*, Eur. Phys. J. **C15** (2000) 1.

[35] M. Amenomori *et al.*, Proc. 25th ICRC (Rome, 1995), vol.4, 1148.

[36] N.A. Tsyganenko, J. Geophys. Res., **100** (1995), 5599

[37] N.A. Tsyganenko and D.P. Stern, J. Geophys. Res., **101** (1996), 27187.

[38] X.-W. Zhou *et al.*, Geophys. Res. Lett., **24** (1997), 1451.

[39] J. Bartels *et al.*, J. Geophys. Res., **44** (1939), 411; data taken from http : //www.ngdc.noaa.gov/stp/GEOMAG/$kp_a$p.html

[40] M. Amenomori *et al.*, Astrophys. J., **464** (1996) 954.

[41] M. Amenomori *et al.*, Astrophys. J., **541** (2000), 1051; M. Amenomori *et al.*, Proc. 27th ICRC (Hamburg, 2001) vol. 9, 3795

[42] M. Chantell *et al.*, Nature, **367**, (1994) 25.

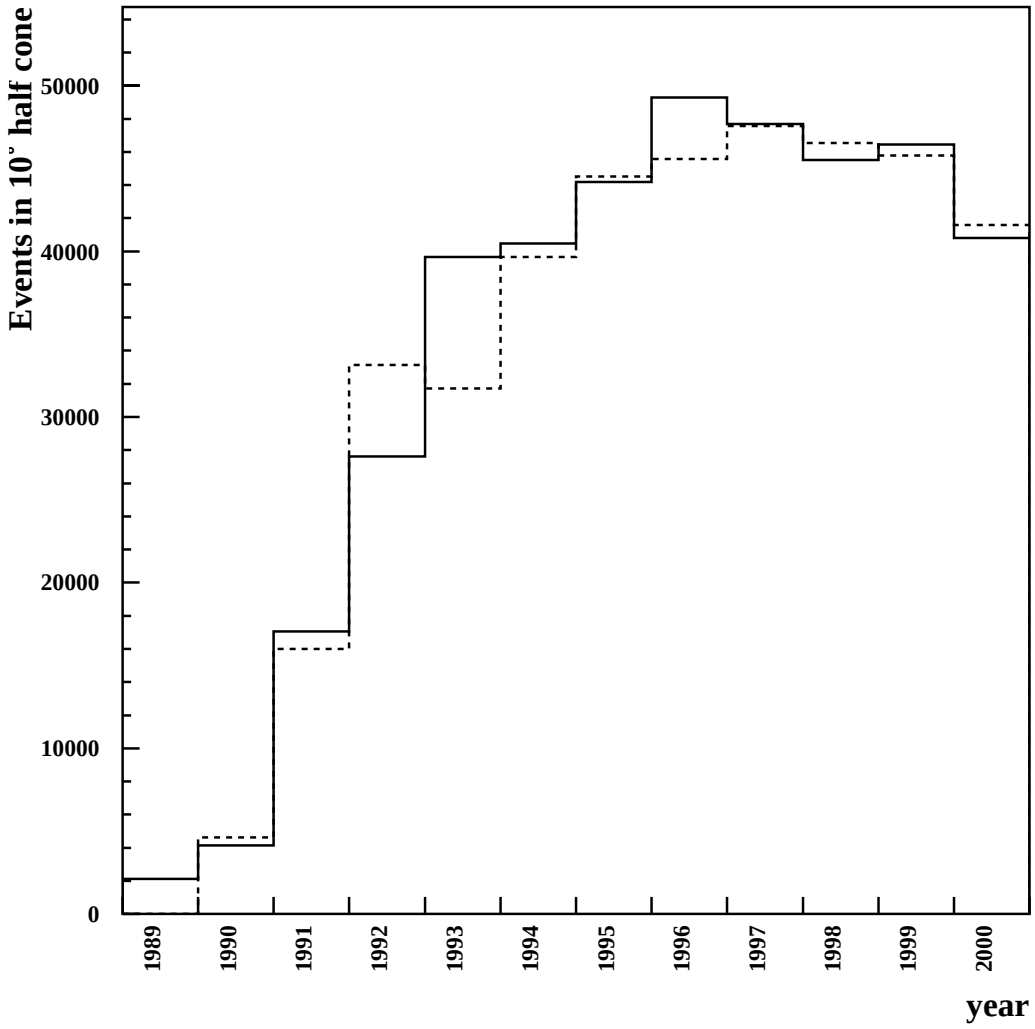


Fig. 1. Number of events in a 10° half-angle cone from the Moon direction (solid histogram) and from the Sun direction (dashed histogram) collected during each year of MACRO data taking.

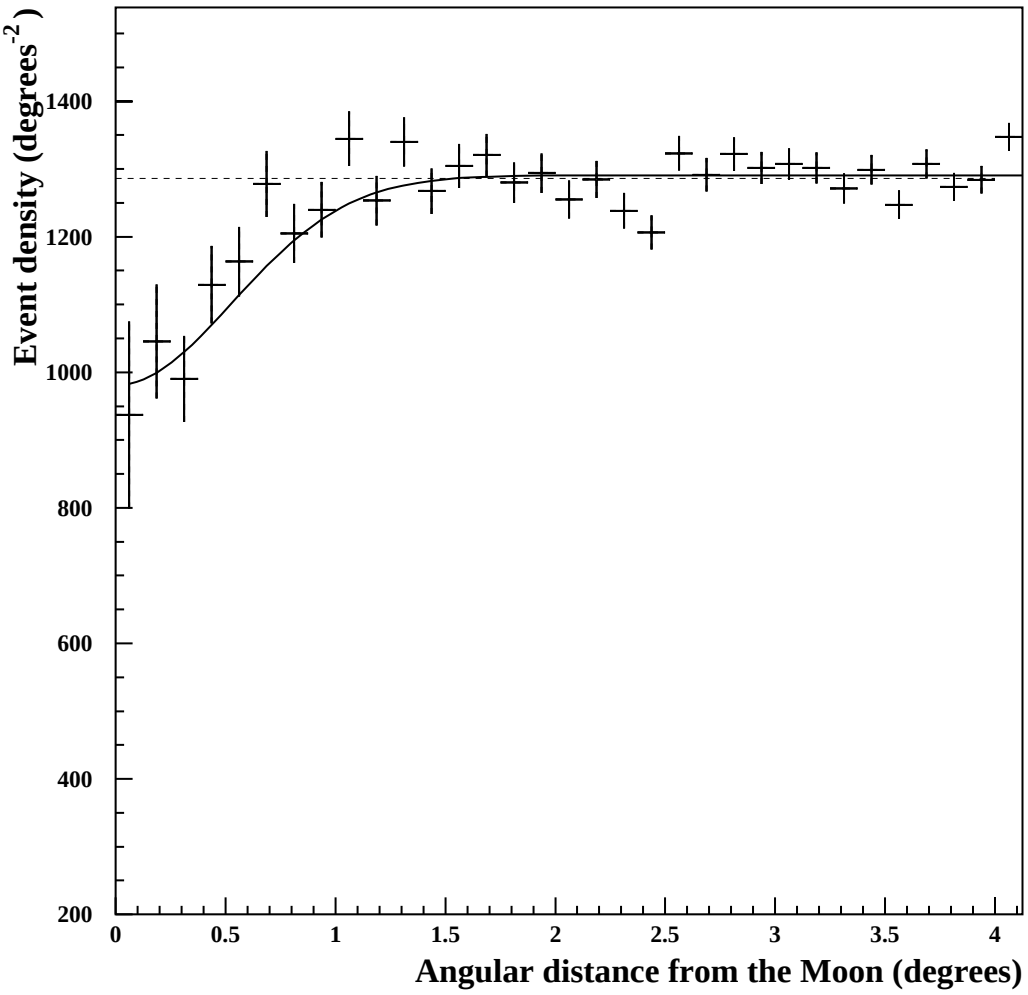


Fig. 2. Event density vs angular distance from the moon center in bins of equal angular width. The width of each bin is 0.125°. The dashed curve is the average expected background computed from 25 background Monte Carlo samples. The solid curve shows the expected event density computed for an angular resolution of the MACRO apparatus in the hypothesis of a PSF normally distributed. The resolution value from the fit is $0.55^\circ \pm 0.05^\circ$ .

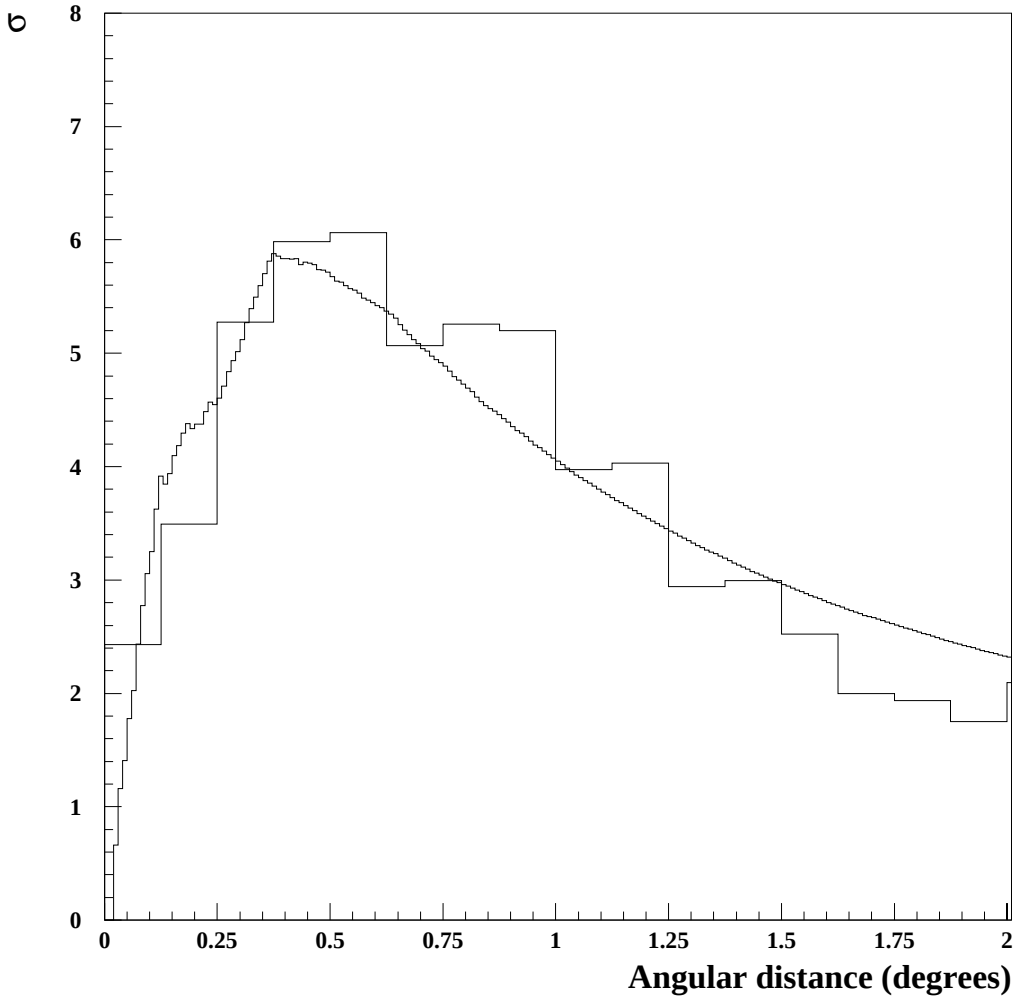


Fig. 3. Deviation from the expected number of events computed as $\sigma = \frac{N_{exp}-N_{obs}}{\sqrt{N_{exp}}}$ versus the angular distance from the Moon center. Superimposed (continuous line) the simulated distribution of the deviations expected using the modified psf distribution for an extended source of 0.26° radius.

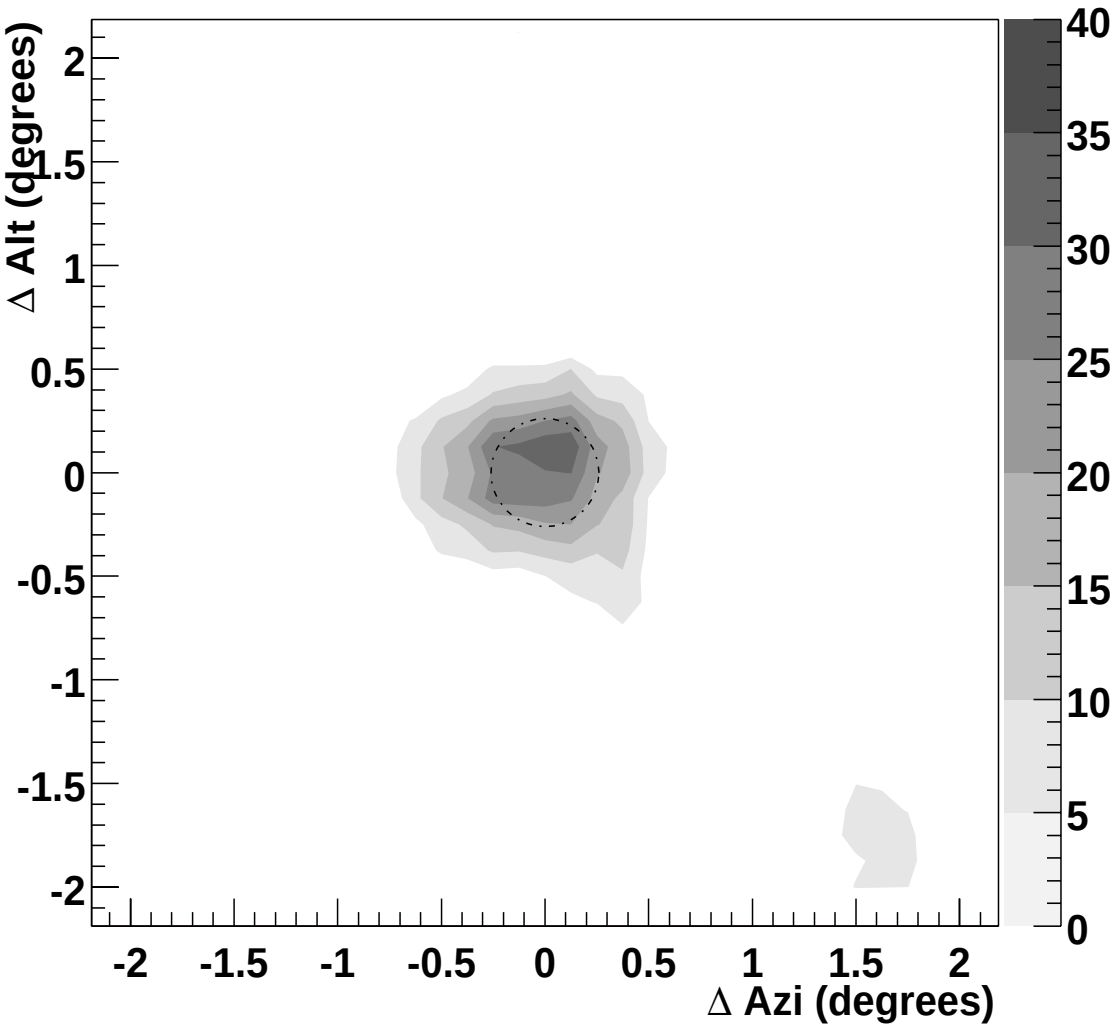


Fig. 4. The two dimensional distribution of $\chi^2$ in bins of equal solid angle in the moon window. The axes are offsets from the moon center. A circle corresponding to the average lunar radius, 0.26°, is centered on the fiducial position of the moon, at position (0,0). The $\chi^2$ grey scale is given at the right margin of the figure. The maximum of this distribution, $\chi^2 = 39.7$, is within the fiducial moon position at $\Delta$ Azimuth $= 0.^\circ$ , and $\Delta$ Altitude $= +0.125^\circ$ . The bin width is $0.25^\circ$ .

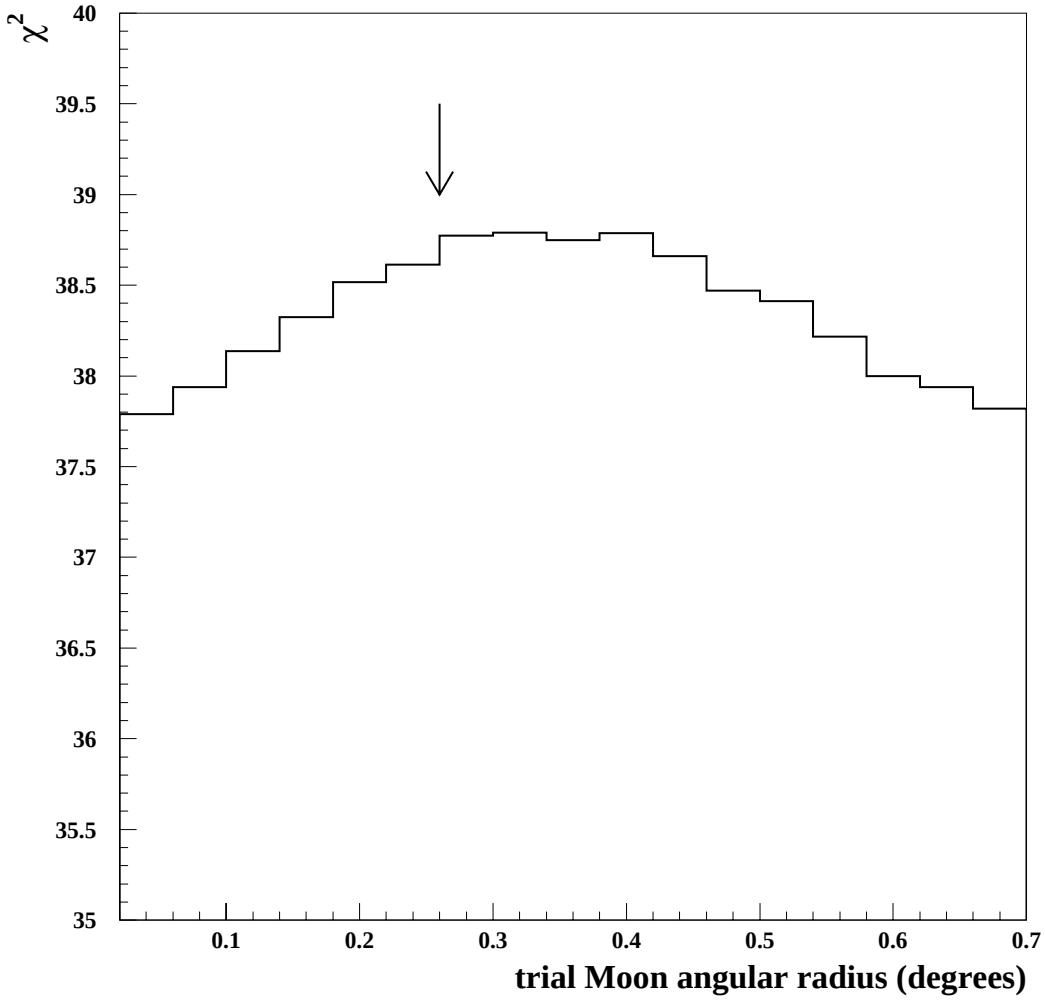


Fig. 5. Distribution of $\chi^2$ values at the Moon shadow center versus the trial angular size for the Moon radius. The interval $\chi^2_{max} - 1$ establishes the error interval for the Moon angular radius. The arrow shows the expected average value for the Moon radius.

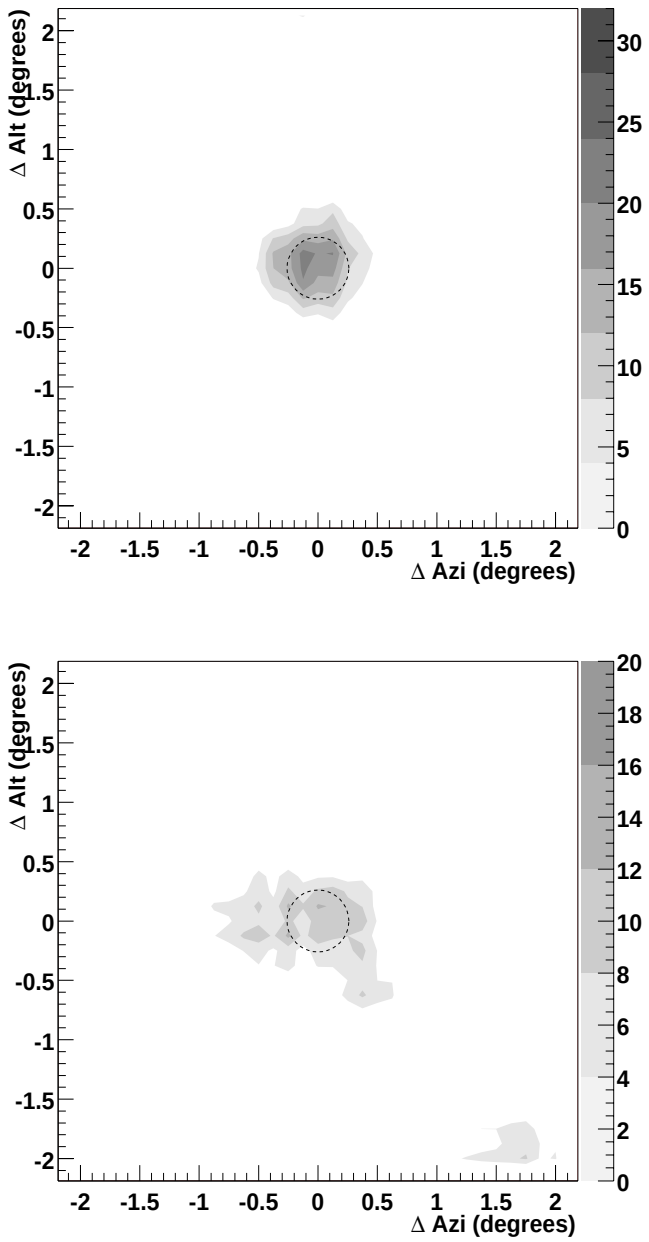


Fig. 6. The two dimensional distribution of $\chi^2$ in bins of equal solid angle in the moon window for the "night" (a) and "day" (b) subsamples. The axes are offsets from the moon center. A circle corresponding to the average lunar radius, 0.26°, is centered on the fiducial position of the moon, at position (0,0). The $\chi^2$ grey scale is given at the right margin of the figure. (a) The maximum of the distribution, $\chi^2 = 25$, is within the fiducial moon position at $\Delta$ Azimuth $= -0.1^\circ$ and $\Delta$ Altitude $= +0.^\circ$ . (b) The maximum of the distribution, $\chi^2 = 17.1$, at $\Delta$ Azimuth $= -0.25^\circ$ and $\Delta$ Altitude $= +0.^\circ$ .

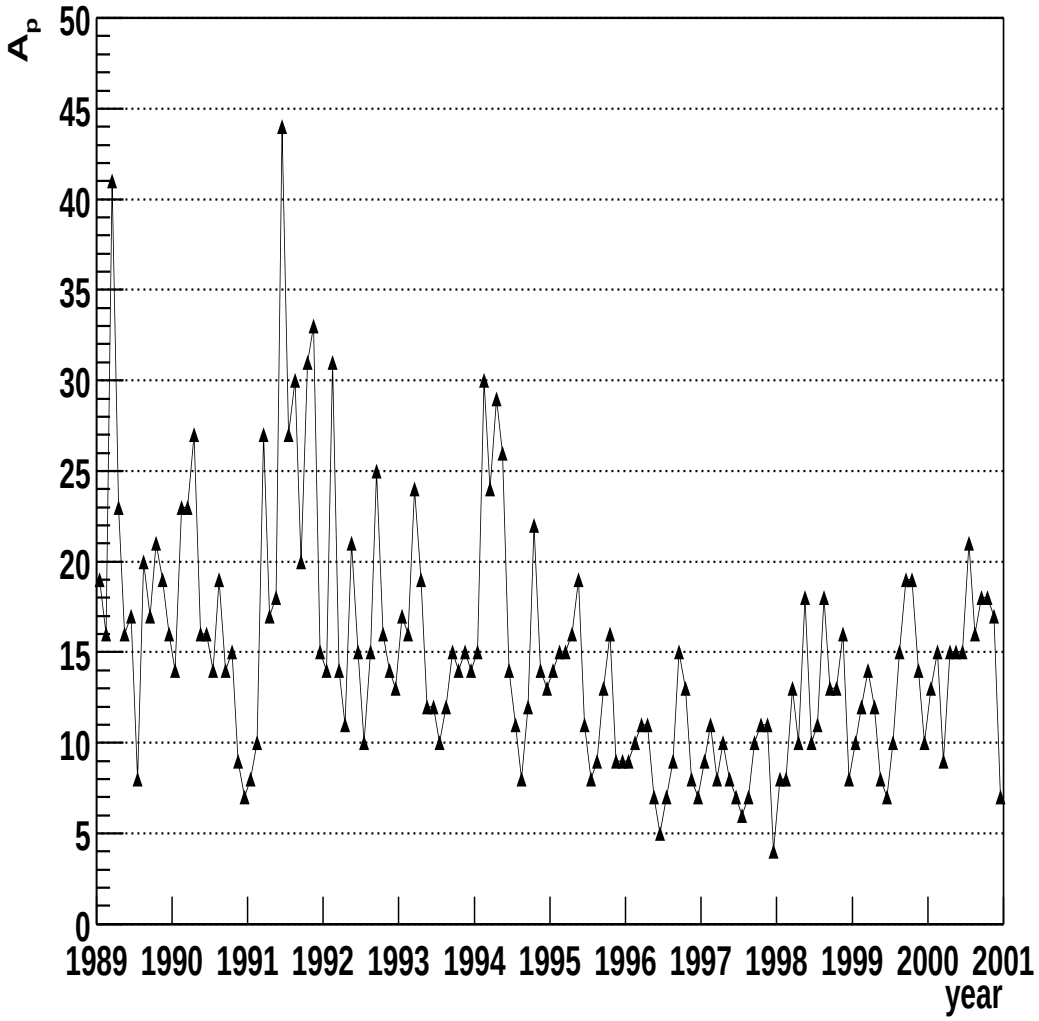


Fig. 7. Monthly $A_p$ index in the 1989-2001 period.

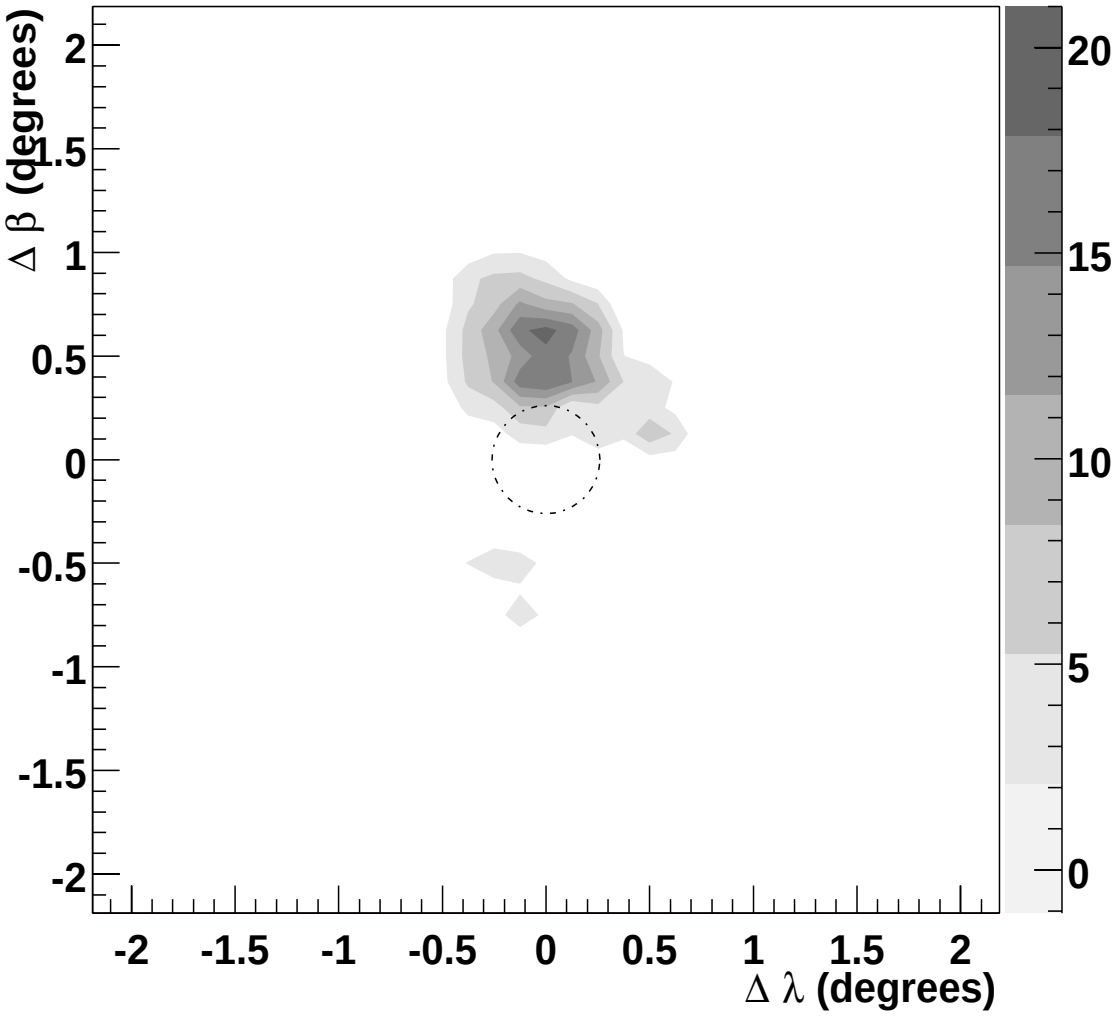


Fig. 8. The two dimensional distribution of $\chi^2$ in bins of equal solid angle in the Sun window in ecliptic coordinates. The axes are offsets from the Sun center. A circle corresponding to the average sun radius, 0.26°, is centered on the fiducial position of the Sun, at position (0,0). The $\chi^2$ grey scale is given at the right margin of the figure. The maximum of this distribution, $\chi^2 = 22.0$, in the position at $\Delta\lambda = 0°$ in longitude and $\Delta\beta = +0.625°$ in latitude. The bin width is 0.25° .

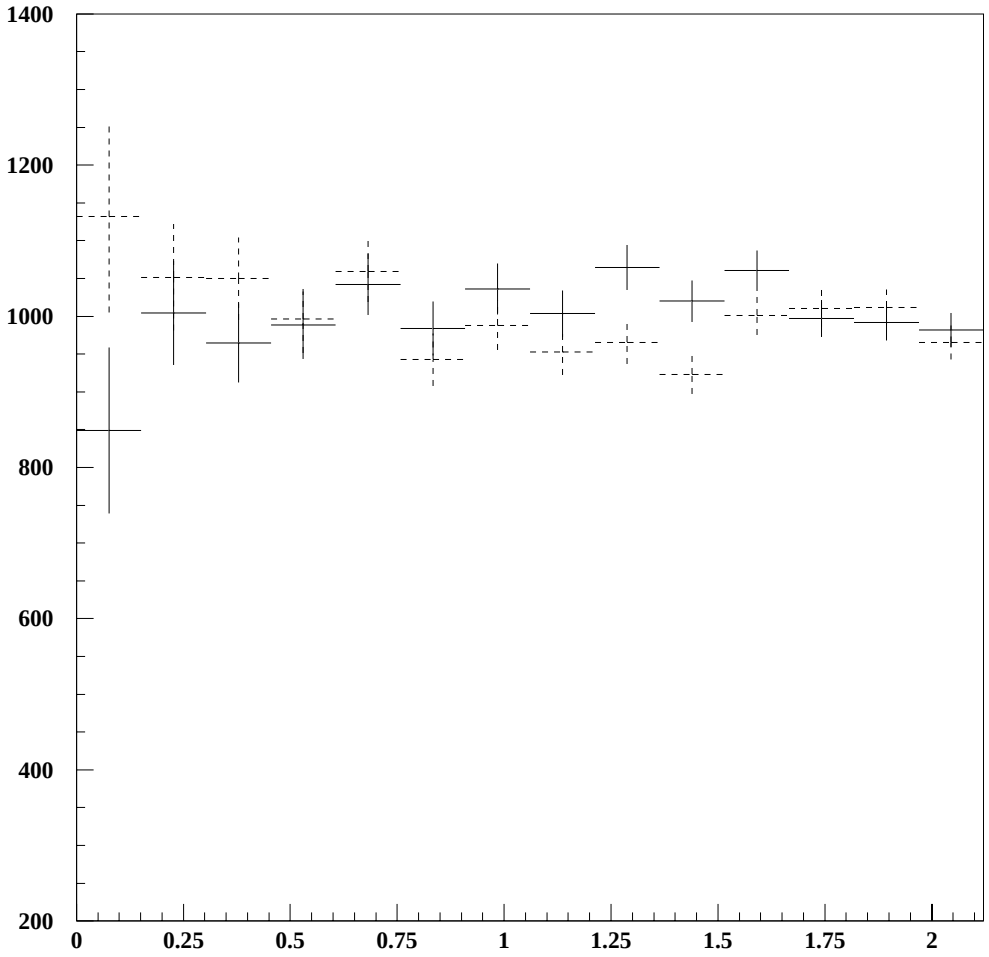


Fig. 9. Event density vs the angular distance from the Sun shadow position (0.6° northward with respect to the "nominal center"). Superimposed the event density distribution centered in the symmetric position 0.6° southward.

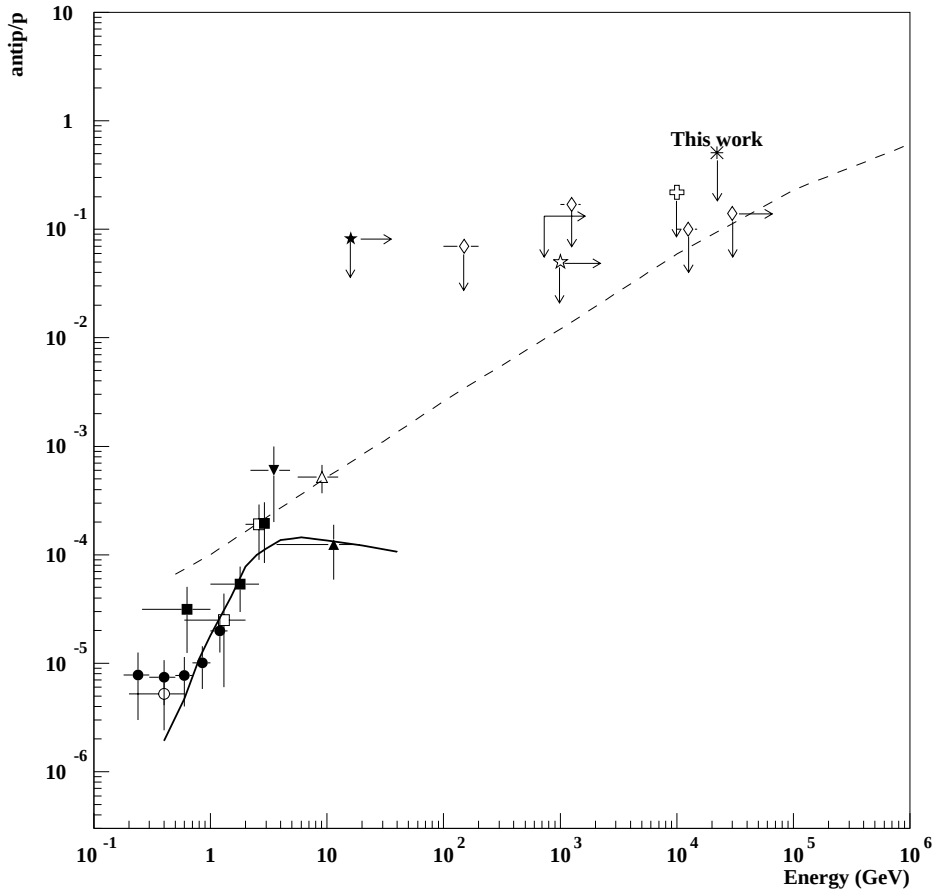


Fig. 10. Antiproton/proton ratio from various experiments at different average energies for period of A>0: △ R.L. Golden et al., Phys. Rev Lett. 43(1979) 1196; ▼ E.A. Bogomolov et al. Proc. 16th ICRC (Kyoto,1979) vol. 1,330; ▲ M. Hof et al. (MASS Collaboration) Astrophys. J., 467 (1996) L33; ■ J.W. Mitchell et al. (IMAX Collaboration) Phys. Rev. Lett. 87 (1996) 3057; ○ K. Yoshimura et al. (BESS Collaboration) Phys. Rev. Lett. 75 (1995); 3792 and A. Misseev et al. (BESS Collaboration) Astrophys. J. 474 (1997) 479; □ M. Boezio et al. (CAPRICE Collaboration) Astrophys. J. 487 (1997) 415; ● H. Matsunaga et al. (BESS Collaboration) Phys. Rev . Lett. 81 (1998) 4052; ✰ G. Brooke and A.W. Wolfendale, Nature, 202 (1964) 480; ★ N. Durgaprasad and P.K. Kunte, Nature, 234 (1971) 74; ◇ S.A. Stephens, Astron. Astrophys., 149 (1985) 1; ✞ [35]; no symbol [16]; ∗ MACRO this work. Solid line: unmodulated intestellar prediction. S.H. Geer and D.C. Kennedy, Astrphys. J. 532 (2000) 348 Dashed line: calculated antip/p ratio for extragalactic origin S.A. Stephens and R.L. Golden, Space Sci. Rev. 46 (1987)